Traffic 2006; 7: 416–428
Blackwell Munksgaard

doi: 10.1111/j.1600-0854.2006.00394.x

Differential Properties of GTP- and Ca^{2+}-Stimulated Exocytosis from Large Dense Core Vesicles

Li Bai[1,a], Dan Zhu[1,a], Keming Zhou[1,a], Wei Zhou[1], Dongdong Li[1], Yan Wang[2], Rongying Zhang[1] and Tao Xu[1,2,*]

[1]Joint Laboratory of Institute of Biophysics & Huazhong University of Science and Technology, College of Life Science and Technology, Huazhong University of Science and Technology, Wuhan 430074, China
[2]National Laboratory of Biomacromolecules, Institute of Biophysics, Chinese Academy of Sciences, Beijing100101, China
**Corresponding author: xutao@ibp.ac.cn*

Many cells utilize a GTP-dependent pathway to trigger exocytosis in addition to Ca^{2+}-triggered exocytosis. However, little is known about the mechanism by which GTP triggers exocytosis independent of Ca^{2+}. We used dual-color evanescent field microscopy to compare the motion and fusion of large dense core vesicles stimulated by either mastoparan (Mas) in Ca^{2+}-free conditions or high K^+ in the presence of Ca^{2+}. We demonstrate that Mas is hardly effective in triggering the fusion of the predocked vesicles but predominantly mobilizes cytosolic vesicles. In contrast, Ca^{2+}-dependent exocytosis is largely due to predocked vesicles. Fusion kinetics analysis and carbon-fiber amperometry reveal that Mas induces a brief 'kiss-and-run' fusion and releases only a small amount of the cargo, whereas Ca^{2+} stimulates a more persistent opening of the fusion pore and larger release of the contents. Furthermore, we show that Mas-released vesicles require a much shorter time to reach fusion competence once they approach the plasma membrane. Our data suggest the involvement of different mechanisms not only in triggering and fusion but also in the docking and priming process for Ca^{2+}- and GTP-dependent exocytosis.

Key words: calcium, fusion, GTP, large dense core vesicles, mastoparan

Received 1 November 2005, revised and accepted for publication 3 January 2006, published on-line 6 February 2006

Exocytosis requires the sequential docking, priming, triggering, and fusion of a single secretory vesicle to release its contents into the extracellular space. When an intracellular vesicle is destined to undergo exocytosis, it first needs to recognize the target plasma membrane by physical contact in a specific location. The tethering or docking of the fusion-prone vesicle to the target membrane provides specificity to the fusion reaction. It is believed that docked vesicles require a further priming step before they can fuse with the plasma membrane. It has been suggested that SNARE complex (1) formation *in trans* may constitute the molecular priming event. SNARE complex formation is thought to bring the vesicle membrane in proximity to the plasma membrane, which might be essential for subsequent fusion (2,3). Consistent with this idea, the size of the readily releasable pool (presumably primed vesicles) is strictly dependent on the formation of the SNARE complex (4–6).

The molecular basis by which the primed vesicles are trigged to fuse is not fully understood. Ca^{2+} plays a pivotal role in the triggering of fusion by binding to the specific Ca^{2+} sensor(s), presumably synaptotagmin via its two C2-domains (7,8). One hypothesis is that the SNARE complex assembly creates a metastable fusion intermediate, perhaps a stalk-like state. Ca^{2+}-triggered insertion of the synaptotagmin C2-domains thus destabilizes the intermediate state and triggers membrane fusion (9).

Accumulating evidence suggests the presence of a Ca^{2+}-independent exocytosis in addition to the well-characterized Ca^{2+}-triggered exocytosis. For example, the degranulation in haematopoietic cells depends on G proteins (10,11). Also, the nonhydrolyzable GTP analogue GTPγS has been shown to induce exocytosis in the absence of Ca^{2+} in secretory cells, including mast cells (10,12), chromaffin cells (13,14), melanotrophs (15), pituitary gonadotrophs (16), pancreatic β cells (17), and platelets (18). Furthermore, mastoparan (Mas), a toxin from wasp venom, has been shown to elicit exocytosis under Ca^{2+}-free conditions in adrenal chromaffin cells (19), platelets (20), mast cells (21), pancreatic β cells (22,23), and pulmonary alveolar type 2 cells (24). Mas stimulates the guanine nucleotide exchange activity of heterotrimeric G proteins as well as low molecular weight G proteins (25–27).

The molecular events involved in Ca^{2+}-independent, G-protein stimulated exocytosis remain largely elusive. The elucidation of the mechanism by which Mas triggers membrane fusion in the absence of Ca^{2+} will contribute to our understanding of the biophysical basis of fusion initiation. Here, by employing Mas and high K^+ to stimulate exocytosis from PC12 cells, we compare single-vesicle exocytosis in response to Ca^{2+}-dependent and Ca^{2+}-independent stimuli and investigate the mechanism underlying GTP-dependent and Ca^{2+}-independent triggering of exocytosis.

[a] These authors contributed equally to the work.

Results

Identification of large dense core granules by co-localization of VAMP2-pHluorin and neutropeptide-Y-DsRed

Monitoring exocytosis with a sole EGFP reporter protein can be problematic due to the low detection rate of EGFP fluorescence (28) and the complex diffusion kinetics of released and membrane-bound EGFP following fusion (28,29). Ecliptic pHluorin is brightly fluorescent at pH 7.4 and is essentially nonfluorescent at about pH $<$ 6.0 (30). Attached to the C terminal of VAMP2, a vesicular membrane protein, it is located in the vesicle lumen where it is exposed to fusion-related pH changes from between 5.0 and 6.0 before fusion (28,30) to neutral pH thereafter. It is thus advantageous to employ VAMP2-pHluorin to monitor the occurrence of vesicle fusion, as the fluorescence of VAMP2-pHluorin is expected to increase dramatically upon exposure of the vesicle lumen during fusion. However, VAMP2-pHluorin is not a specific marker of one type of vesicles, as it can be sorted to both large dense core granules (LDCVs) and synaptic-like vesicles. Also, it is difficult to obtain information about the pre- and post-exocytotic steps from vesicles labeled with VAMP2-pHluorin due to the rapid quenching of fluorescence in the acidic and re-acidified vesicular lumen. In contrast, neutropeptide-Y (NPY)-EGFP has been used successfully to specifically label LDCVs in PC12 cells (31). Hence, for simultaneous imaging of NPY with VAMP2-pHluorin, we constructed NPY-DsRed. Figure 1A shows the co-localization of NPY-DsRed with NPY-EGFP. We estimate that 89.6% of the NPY-DsRed spots are co-localized with NPY-EGFP fluorescence. By simultaneous dual-color imaging of VAMP2-pHluorin and NPY-DsRed fluorescence, we found that the fusion events of LDCVs can be reliably detected, and the pre- and post-exocytotic stages can be monitored via tracking of NPY-DsRed fluorescence, because DsRed is less sensitive to pH. To verify the co-localization of the two fluorescent proteins, we co-transfected plasmids containing VAMP2-pHluorin and NPY-DsRed into PC12 cells. After perfusion of 50 mM NH_4Cl to alkalize the vesicle lumen, VAMP2-pHluorin fluorescence was partially (74.7%, $n = 253$) co-localized with the LDCV marker NPY-DsRed (Figure 1B). We also observed VAMP2-pHluorin-reported fusion events from fluorescence in the absence of NPY-DsRed labeling. Apparently, some of the VAMP2-pHluorin may also be sorted to the synaptic-like microvesicles in PC12 cells.

Monitor fusion of LDCVs induced by Mas

Mas has been previously shown to cause Ca^{2+} elevation (22). We have verified that Mas induces significant $[Ca^{2+}]_i$ elevation in the presence of extracellular Ca^{2+} (2.6 mM) but not in the external solution lacking Ca^{2+} (data not shown), suggesting the source of $[Ca^{2+}]_i$ elevation is mainly due to Ca^{2+} influx. Hence, all of our experiments were carried out in a Ca^{2+}- and Mg^{2+}-free external solution containing 1 mM EGTA, where Mas (10 μM) induces vigorous exocytosis. Figure 2A shows an example exocytotic event observed under dual-color total internal reflection fluorescence microscopy (TIRFM). We observed a sudden and brief brightening of a fluorescence spot in the green channel (pHluorin fluorescence). At the corresponding position in the red channel (DsRed fluorescence), there was a concurrent appearance of a fluorescence spot. Figure 2A shows the evolution over time of both the green and red images in the upper traces of Figure 2B. We interpret the sudden increase in the pHluorin fluorescence as a fusion event, because lumenal pHluorin only increases in brightness when encountering the neutral pH of the external medium during fusion pore opening. Two other fusion events are also displayed in Figure 2B. It is of interest to note that the DsRed fluorescence continues to increase even after the increase in the pHluorin fluorescence. This increase can only partially be explained by the shift of pH in the vesicle, because DsRed is virtually insensitive to pH (pKa = 4.7) (32). It is possible that there is a further approaching of the dense core inside the vesicle toward the cell surface after the initial fusion pore dilation, or the alkalinization of the inside of secretory vesicles can occur right before exocytosis, as previously suggested (33).

After fusion, the pHluorin fluorescence was usually maintained at the peak value for only 1–2 frames and then fell

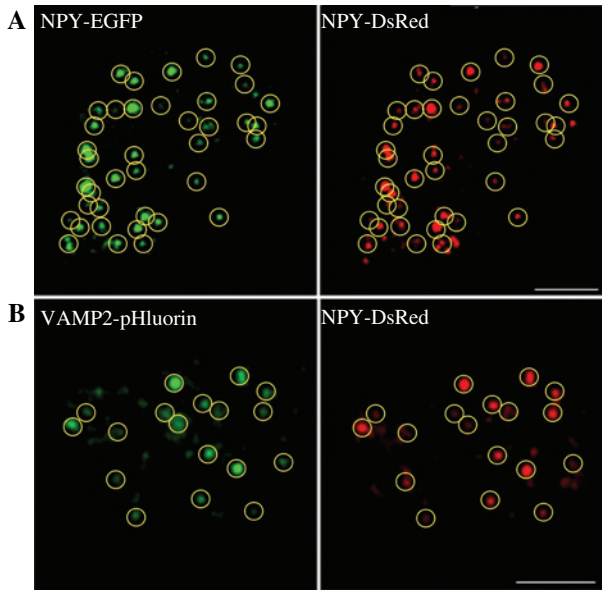

Figure 1: Fluorescent labeling of large dense core granules in PC12 cells. Upper images: Co-localization of neutropeptide-Y (NPY)-DsRed and NPY-EGFP revealed by dual-color imaging under total internal reflection fluorescence microscopy (TIRFM). Bottom images: Co-localization of VAMP2-pHluorin and NPY-DsRed revealed using dual-color imaging under TIRFM. Yellow circles indicate co-localized vesicles. Cells were treated with 50 mM NH_4Cl to brighten the VAMP2-pHluorin fluorescence by alkalization of the vesicle lumen. The scale bar indicates 5 μm.

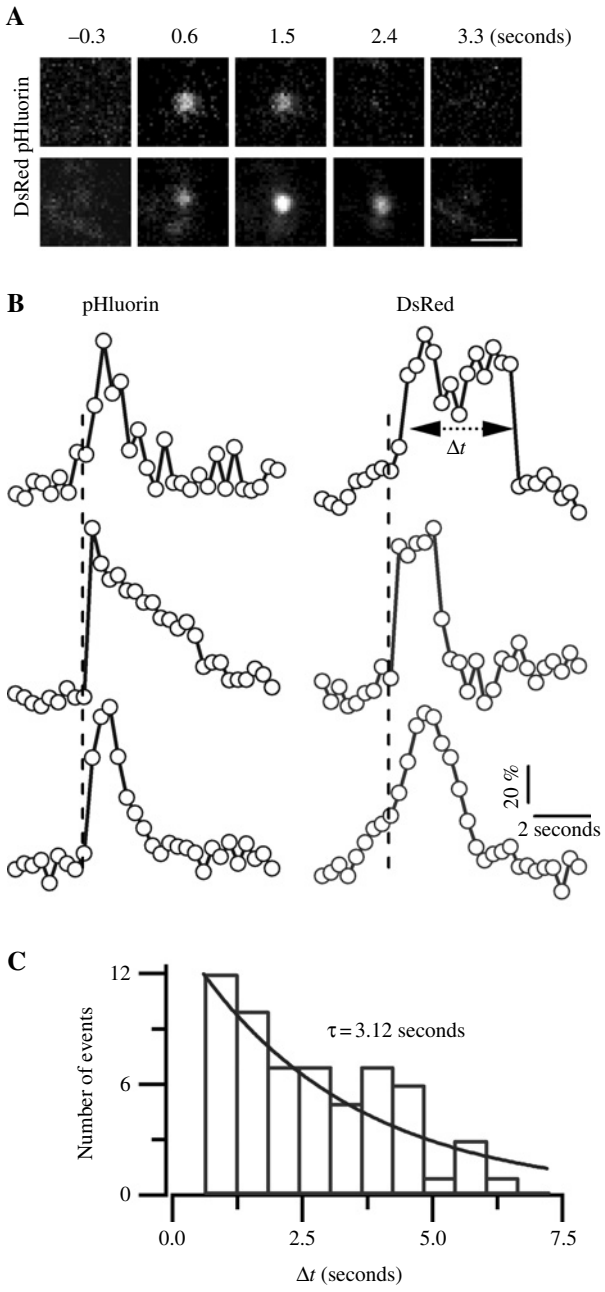

Figure 2: Monitoring exocytosis of large dense core granules (LCDVs) triggered by mastoparan. (A) Sequential images of a single LDCV labeled with both VAMP2-pHluorin and NPY-DsRed undergoing exocytosis. The time indicated is relative to the onset of fusion. The scale bar represents 1 μm. (B) Time courses of three example fusion events. Upper traces correspond to the vesicle in A. Fluorescence intensities were averaged from 1-μm diameter circles enclosing the vesicles after background subtraction and expressed as the percentage of the peak fluorescence. Vertical dashed lines indicate the time of fusion inferred from the VAMP2-pHluorin fluorescence. (C) Distribution of the dwelling time of LDCVs at the plasma membrane after fusion. The dwelling time (Δt) was measured between the peak of the pHluorin fluorescence and the point where the DsRed fluorescence fell to 50% of its peak.

rapidly, suggesting a transient opening of the fusion pore for <0.4 seconds followed by its rapid closure. The dimming of the pHluorin fluorescence could possibly be due to the re-acidification of the vesicle lumen after exocytosis. In contrast, the DsRed fluorescence remained for a certain time even after the closure of the fusion pore. Eventually, the punctuate DsRed fluorescence declined as it moved out of the evanescent field. We measured the time difference (Δt) between the peak of the pHluorin fluorescence and the point where the DsRed fluorescence declined to its half-maximal value, which should reflect the dwell time that the vesicle spends in the fusion state. The distribution of Δt follows a monoexponential function with a time constant of 3.12 seconds (Figure 2C). We conclude that, on average, LDCVs dwelled for some 3 seconds at the plasma membrane after transient fusion before being retrieved to deeper cytoplasmic regions not illuminated by the evanescent field.

Figure 3A shows a latency histogram of exocytotic events triggered by Mas. Mas-induced fusion was less synchronized than Ca^{2+}-dependent exocytosis. Unlike Ca^{2+}-triggered exocytosis that showed a biphasic rapid onset and sustained rate of exocytosis (see Figures 4 and 5), the rate of Mas-triggered exocytosis reached a peak after approximately 20 seconds and fell slowly after the application of Mas was stopped. Mas-induced exocytosis was not inhibited by emptying the Ca^{2+} store with thapsigargin pretreatment (2 μM for 15 min, supplementary Figure 1), suggesting that intracellular Ca^{2+} release is not involved. Fusion events rarely occurred before Mas stimulation (Figure 3A), so we conclude that the exocytosis observed here is a triggered event independent of Ca^{2+}. Mas is an amphiphilic tetradecapeptide that inserts into the phospholipid bilayer of the plasma membrane. To exclude the possibility that Mas triggers exocytosis simply by physical perturbation of the plasma membrane, and to better understand the nature of Mas-induced exocytosis, we used Mas-17, an inactive analog of Mas that does not activate G proteins. As shown in Figure 3B, 50 μM Mas-17 fails to trigger significant exocytosis. In addition, to confirm that Mas-induced exocytosis requires SNARE proteins, we transfected a plasmid encoding the light chain of botulinum neurotoxin type E (BoNT/E). Indeed, cleaving SNAP-25 and impairing SNARE complex assembly (34) significantly reduced Mas-induced exocytosis (Figure 3B). The incomplete inhibition of exocytosis by BoNT/E might be due to the low expression levels or incomplete proteolysis by BoNT/E.

Whereas Ca^{2+} preferentially releases the docked vesicles first, we were surprised to find the majority of visible vesicles did not undergo exocytosis in response to Mas stimulation. We define vesicles that are present during the entire 10 seconds before stimulation as 'visible' and those that are absent 10 seconds before stimulation and only enter the evanescent field during stimulation as 'newcomers'. We observed that most Mas-related fusion

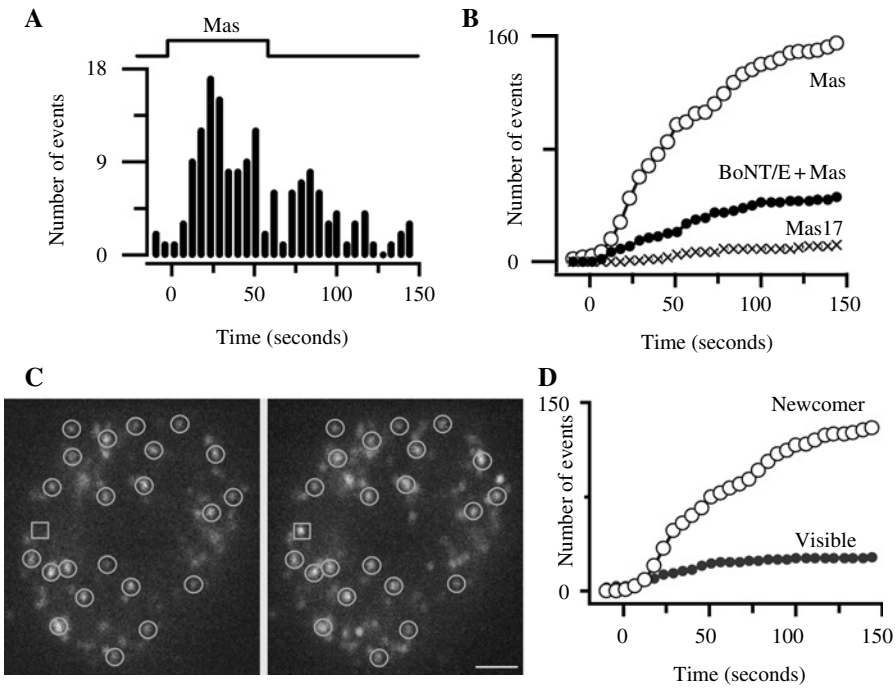

Figure 3: Mastoparan (Mas) fails to trigger the fusion of predocked vesicles. (A) The number of fusion events is plotted against time relative to Mas (10 μM) application. (B) Cumulative numbers of total fusion events plotted against time from cells treated with Mas (open circle) or Mas17 (50 μM). Also compared are Mas-induced fusion events from cells transfected with botulinum neurotoxin type E (BoNT/E) (BoNT/E + Mas). VAMP2-pHluorin was cotransfected with BoNT/E light chain 3 days prior to the experiments. (C) Comparison of the footprint of a live PC12 cell under evanescent-field illumination 10 seconds before (left) and after (right) the application of Mas. The right image was averaged from three images taken at 51, 60.3, and 71.7 seconds after Mas application. The visible vesicles are outlined by circles. One newcomer is indicated by the square box. Scale bar represents 2 μm. (D) Cumulative number of fusion events plotted against time after perfusion of Mas. Vesicles that were visible for 10 seconds before the application of Mas were defined as visible vesicles. The remaining vesicles were considered as newcomer vesicles.

events were supported by 'newcomers'. Figure 3C shows the images taken before (left) and after (right) Mas application. Most vesicles visible before stimulation (circles in Figure 3C) are still observed 1 min after Mas application. In Figure 3D, we compared the cumulative fusion events from visible and newcomer vesicles, respectively, showing that Mas-induced exocytosis is largely due to newcomers. We estimated that 17% of the Mas-induced exocytosis was from visible vesicles and the remaining 83% was from newcomers. This is in stark contrast to Ca^{2+}-evoked exocytosis where the majority (92%) of release comes from visible vesicles, as shown in Figure 5 (see also 35,36). To quantify the mobility of vesicles, we calculated their 3-D diffusion coefficients ($D^{(3)}$) based on the least-square fits to the mean square displacement (MSD) as a function of time (37,38). We found that most of the visible vesicles have a $D^{(3)} < 5 \times 10^{-4}$ $\mu m^2/s$, which is comparable with the 'docked' vesicles defined in previously studies (39,40), suggesting that the majority of visible vesicles are composed of docked vesicles. The average 3-D diffusion coefficient of the visible vesicles that are released upon Ca^{2+} elevation is $(1.2 \pm 0.1) \times 10^{-4}$ $\mu m^2/s$, much smaller than that of the newcomers released upon Mas $(9.0 \pm 2.5) \times 10^{-4}$ $\mu m^2/s$. It should be noted that the release rate of predocked vesicles in the presence of Mas is similar to that of spontaneously occurring fusion events with no stimulation (see Figure 3A). Thus, Mas appears to preferentially target undocked vesicles.

Mas spares the burst component of exocytosis triggered by flash photolysis

To further confirm the observation that Mas does not release predocked vesicles, we investigated the effects of Mas on exocytosis triggered by flash photolysis of caged Ca^{2+} [DM-nitrophen (DMN)]. Exocytosis was assayed using high time-resolution membrane capacitance measurements. The homogenous step-like elevation of $[Ca^{2+}]_i$ in response to the UV flash elicited a rapid burst-like membrane capacitance (Cm) increase followed by a slow sustained component (Figure 4A). The burst component is generally interpreted as the fusion of docked and primed vesicles, whereas the sustained component represents the release of vesicles that were in earlier maturation stages at the onset of stimulation (41). It has been suggested that the sustained component involves recruitment from a docked but unprimed pool (41). Employing live cell TIRFM imaging, it has been

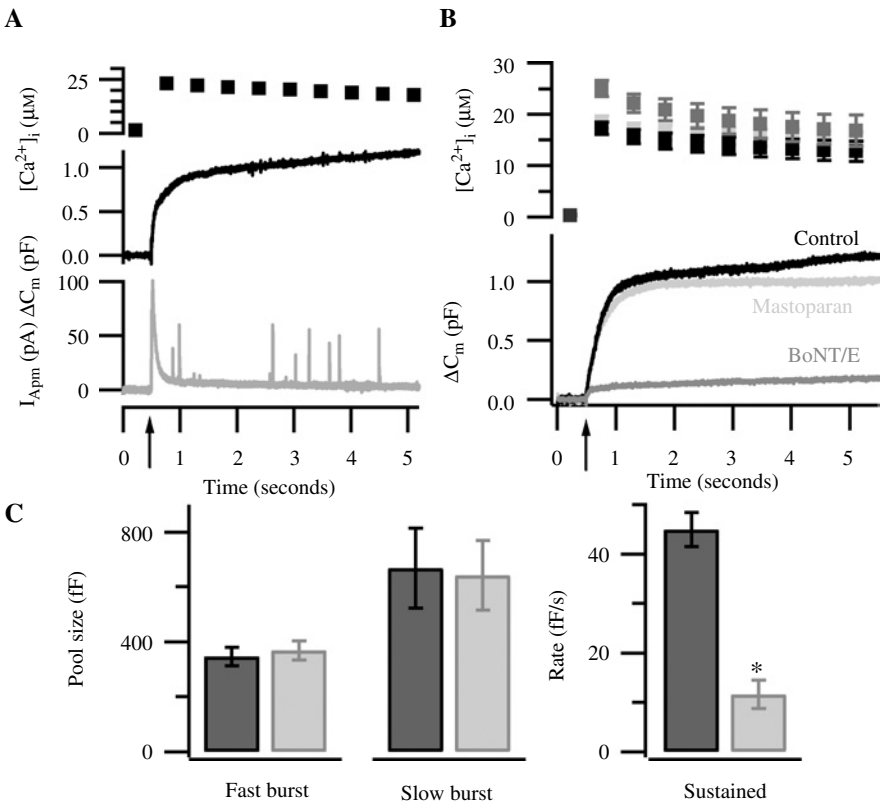

Figure 4: Mastoparan (Mas) suppresses the sustained component of exocytosis. (A) Example Cm response to flash photolysis and the accompanying amperometric signal from the same cell. Arrow indicates the flash time. (B) Shown are averaged $[Ca^{2+}]_i$ (upper panel; error bars represent SEM) and Cm responses (lower panel) to flash photolysis of caged Ca^{2+} from control cells (black, $n = 10$), Mas (10 μM) treated cells (light gray, $n = 13$), and cells transfected with botulinum neurotoxin type E (BoNT/E) (dark gray, $n = 14$). (C) Summary of the effect of Mas on different components of exocytosis. The basal $[Ca^{2+}]_i$ levels prior to the flashes were estimated to be around 300 nM using fura-2. No significant differences were observed between burst components of control cells and Mas-treated cells. The Mas-treated cells, however, display a significantly reduced release rate of sustained component compared with the control group. *$p < 0.001$ (Student's *t*-test).

shown that the sustained release also requires capture of undocked vesicles (40,42). We verified that the burst component of Cm increase was due to exocytosis from catecholamine-containing granules from simultaneous measurements using amperometry (Figure 4A) and was sensitive to BoNT/E blockade (Figure 4B). The experiments were performed in Ca^{2+}- and Mg^{2+}-free bath solution with 1 mM EGTA to avoid any Ca^{2+} influx that may be caused by Mas (22). Flashes were triggered after perfusion of 10 μM Mas for 2–3 min. As shown in Figure 4B,C, Mas treatment does not markedly affect the size of the burst component ($n = 13$) as compared with the control condition ($n = 10$). In addition, the time constants of the fast burst and slow burst are not significantly different between control cells ($\tau_{fast} = 58 \pm 7$ ms, $\tau_{slow} = 250 \pm 24$ ms) and Mas-treated cells ($\tau_{fast} = 55 \pm 5$ ms, $\tau_{slow} = 336 \pm 48$ ms), respectively. These results suggest that the docked and primed vesicles are not preferentially targeted by Mas. Interestingly, we also observed a significant reduction in the sustained component. The averaged slope of the sustained component is 45 ± 3 fF/s in control cells and 12 ± 2 fF/s in the presence of Mas (Figure 4C). It is unclear why Mas reduces the sustained component of exocytosis. One possible explanation might be that prolonged stimulation of Mas depletes the reserve pool and hence causes a reduced sustained component. However, an increased endocytosis rate by G-protein activation could equally explain the phenomenon.

Comparison between Ca^{2+}- and GTP-dependent exocytosis

Ca^{2+}-triggered LDCV fusion from PC12 cells has been assayed by monitoring the diffusion and loss of NPY-EGFP or ANF-EGFP fluorescence (29,31,35). However, the detected number of events may underestimate the multiple forms of fusion events, because vesicles that only transiently expose their lumen to the extracellular space do not necessarily lose their entire fluorescent cargo. For example, it has been reported that the fusion events detected using NPY tagged with a yellow fluorescent protein, venus, occurred much less frequently than those detected using VAMP2-pHluorin in pancreatic MIN6 cells (28). Using dual-color detection of VAMP2-pHluorin and NPY-DsRed, we thus studied the Ca^{2+}-dependent fusion induced by high-K^+ depolarization. Figure 5A illustrates a typical fusion event in response to application of 105 mM K^+. The vesicle was visible in the NPY-DsRed channel before stimulation and underwent fusion with the plasma membrane at 23.8 seconds after application of high K^+, as indicated by the concurrent increase in both pHluorin and DsRed fluorescence. While the pHluorin fluorescence rapidly decayed after fusion, the DsRed fluorescence declined much more slowly. In panel 5B, we plot the cumulative number of fusion events for visible and newcomer vesicles. In contrast to the Mas-induced exocytosis, the majority of high-K^+ triggered exocytosis was due to fusion of visible vesicles. This observation is in agreement with previous studies (35,36) and indicates that Ca^{2+} triggered the fusion of docked vesicles.

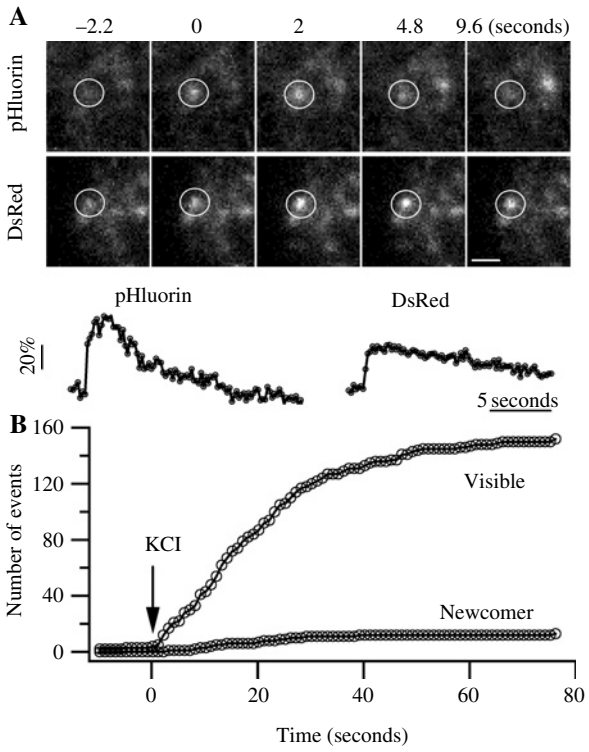

Figure 5: High K^+ preferentially triggers the exocytosis of visible vesicles. (A) Sequential images of a visible large dense core granule (LDCV) labeled with both VAMP2-pHluorin and NPY-DsRed undergoing exocytosis. The scale bar indicates 1 μm. The time indicated is relative to the onset of fusion. Fluorescence intensities (expressed as percentage change) in 1-μm diameter circles (drawn in the graph) are plotted against time below. (B) Cumulative numbers of fusion events plotted against time after elevating K^+. Visible and newcomer vesicles are defined as in Figure 3D.

To determine whether any difference exists in the final fusion reaction between Ca^{2+}- and Mas-induced exocytosis, we compared the averaged time–course of fusion. Figure 6A displays the averaged fusion events stimulated by high K^+ from LDCVs containing both VAMP2-pHluorin and NPY-DsRed. VAMP2-pHluorin fluorescence increased for <1 second and then declined exponentially with a time constant of 4.48 ± 0.21 seconds. Often, we observed VAMP2-pHluorin brightening and rapidly spreading into a cloud as it diffused away into the plasma membrane, as previously shown in chromaffin cells (43) and β cells (28). The diffusion of VAMP2-pHluorin is also seen by the fluorescence increase in the concentric annulus around the central circle (see Figure 6A). Whereas the pHluorin signal increased about sixfold from a very low level [$(F_{peak}$-$F_0)/F_0$] and vanished rapidly after fusion, the NPY-DsRed signal increased only slightly from a much higher level of prefusion fluorescence and diminished slowly with a time constant of 25.38 ± 0.49 seconds. Measurable punctuate NPY-DsRed fluorescence remained at the vesicle sites after fusion, indicating that LDCVs fail to release all of their NPY-DsRed and remain intact after fusion, as previously suggested (29). The tetramerization properties of DsRed may account for the slow diffusion of the protein from the vesicle lumen. The persistence of NPY-DsRed makes it a useful indicator for monitoring vesicles before and after exocytosis. The high prefusion fluorescence of NPY-DsRed is consistent with the conclusion that high K^+ triggers the fusion of docked vesicles underneath the plasma membrane.

In contrast to high K^+-stimulated exocytosis, the kinetics of fusion events triggered by Mas (Figure 6B) reveals striking differences. Firstly, the fluorescence decay is a double exponential, with fast time constants of 0.55 ± 0.03 and 0.28 ± 0.004 seconds and slow time constants of 5.08 ± 0.08 and 6.71 ± 0.16 seconds for pHluorin and DsRed fluorescence, respectively. The fast decay could be due to the rapid closure of the fusion pore and/or re-acidification of the vesicles. The time constants of the slow decay correlate well with the mean dwelling time of vesicles at the plasma membrane (Figure 2C), suggesting that the slow decay might be due to the retreat of vesicles after fusion from the plasma membrane, as we show in Figure 2. Secondly, the fluorescence level of NPY-DsRed before fusion is close to the background fluorescence and much lower than that of high K^+-induced fusion events. Thirdly, no increase in the annulus fluorescence could be observed. These differences further support our above hypothesis that Mas triggers fusion of newly arrived vesicles from the cytosol and that the fusion process seems to be a transient 'kiss-and-run' type with no appreciable diffusion of vesicular membrane protein.

We have shown above that Mas spares the visible vesicles and preferentially triggers the fusion of newcomers. However, it is not known whether newcomer vesicles induced by Mas still need to go through a similar docking and priming step prior to fusion as those triggered by Ca^{2+}. For fusion from newcomers induced by high K^+, we frequently observed a stage at which the DsRed fluorescence stabilized at an intermediate level prior to fusion (Figure 6C). This stage is interpreted as a docking and priming step required for subsequent fusion (36). For Mas-triggered exocytosis, however, a discernable docking and priming stage is hardly visible. Rather, most vesicles fused with the plasma membrane immediately after they appeared (within 1–2 frames) in the red channel (see also Figure 2B). In Figure 6D, we plot the latency histogram of the delay between the first appearance of the vesicle and the fusion event. It is evident that high K^+-induced fusion events have a longer delay time with an exponential decay time constant of 3.95 seconds. In contrast, Mas-induced exocytosis has a much shorter delay. The averaged delay time, which should be equal to the time constant of the exponential fit, is only 0.52 second. This result suggests the existence of different mechanisms not only in fusion triggering but also in the docking process for Mas- and Ca^{2+}-stimulated exocytosis.

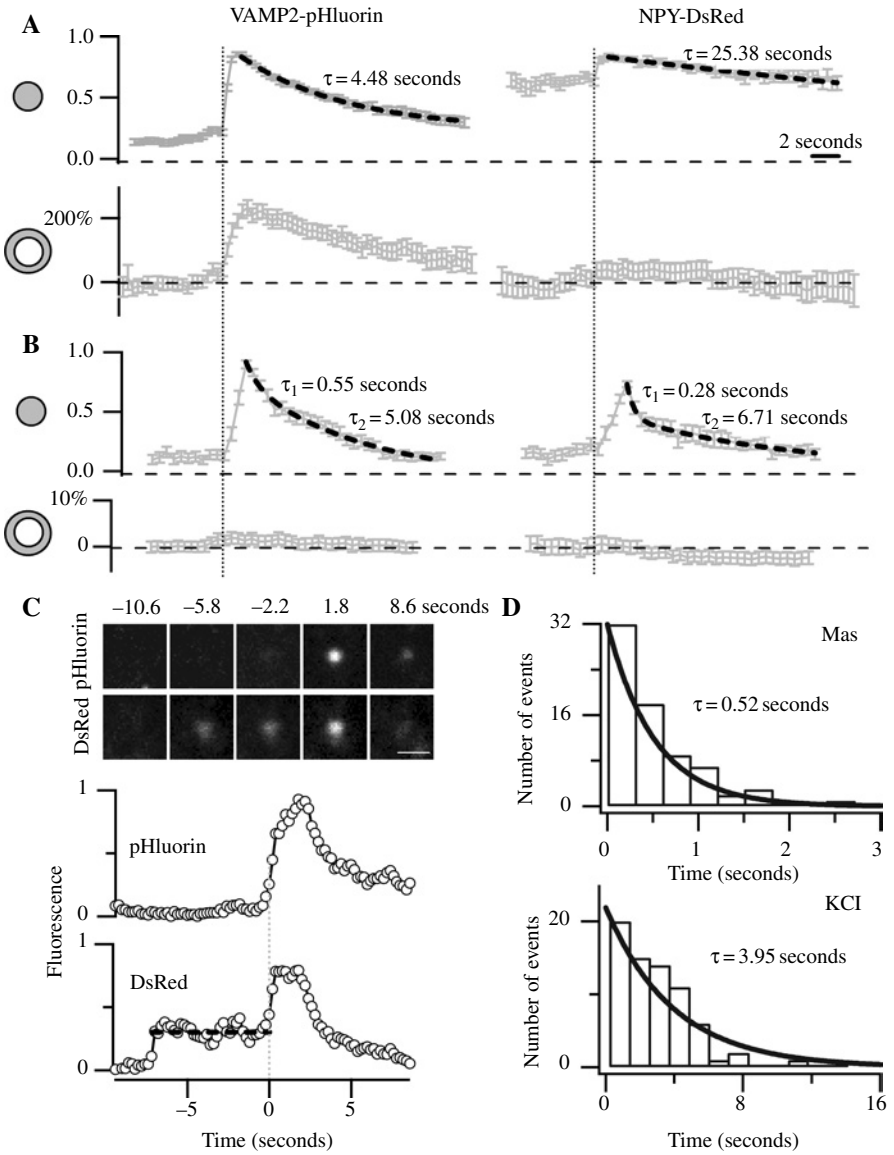

Figure 6: Comparison of the fusion kinetics between high K^+- and mastoparan (Mas)-stimulated exocytosis. Averaged fluorescence traces of large dense core granules (LDCVs) containing both VAMP2-pHluorin and neutropeptide-Y (NPY)-DsRed stimulated by high K^+ (A; 51 events, seven cells) and Mas (B; 27 events, six cells) are displayed. Both the fluorescence intensity from the central circles (1 μm in diameter) enclosing the vesicles and the concentric annuli around the circles (1.5 μm outer diameter) were temporally aligned to the moment of fusion (indicated by the vertical dotted line) as reported using VAMP2-pHluorin. The fluorescence intensity of the central circles was normalized to its peak value. For the concentric annuli, the fluorescence was normalized to the prefusion intensity and expressed as percentage increase. Best exponential fits to the fluorescence decay are superimposed as dashed lines with time constants indicated. Please note the different scale in the lower trace of panel B. (C) Sequential images of a newcomer LDCV labeled with both VAMP2-pHluorin and NPY-DsRed undergoing Ca^{2+}-induced exocytosis. The time indicated is relative to the onset of fusion. Scale bar indicates 1 μm. The fluorescence intensities of the green and red channel were averaged from 1-μm diameter circles enclosing the vesicle and displayed in the bottom. Vertical dotted lines indicate the time of fusion inferred from the VAMP2-pHluorin fluorescence. Please note the apparent docking/priming stage prior to fusion (indicated by broken line). (D) Latency histograms of the delay between the first appearance of vesicles and the fusion time for Mas and Ca^{2+}-induced exocytosis. Superimposed are exponential fits with time constants indicated. Please note the different time scales for the histograms.

If Mas triggers transient 'kiss-and-run' fusion, we would expect to observe a substantial difference in the content release at the single vesicle level between high K^+- and Mas-stimulated exocytosis. We tested this hypothesis by amperometrically detecting the amount of catecholamine release using carbon-fiber electrodes. We challenged PC12 cells with either Mas or high K^+ and examined the characteristics of single fusion spikes. In general,

Mas-induced fusion spikes are much smaller than those induced by high K^+. One example is shown in Figure 7A. Spikes stimulated by high K^+ tend to have larger peak amplitudes (Figure 7B) and longer half times (data not shown), which result in larger content release as judged by the integrated charge of spikes (Figure 7C). The smaller peak amplitudes of Mas-induced spikes could result from partial release due to the brief opening of the fusion pore, as proposed above. Alternatively, it is possible that Mas has limited access to the cleft between carbon fiber and cell, and thus, only spikes from the periphery are measured. However, such distant spikes might have a slower rise time. We have verified that the rise time (10–90%) is not significantly different between high K^+ and Mas-induced spikes (data not shown).

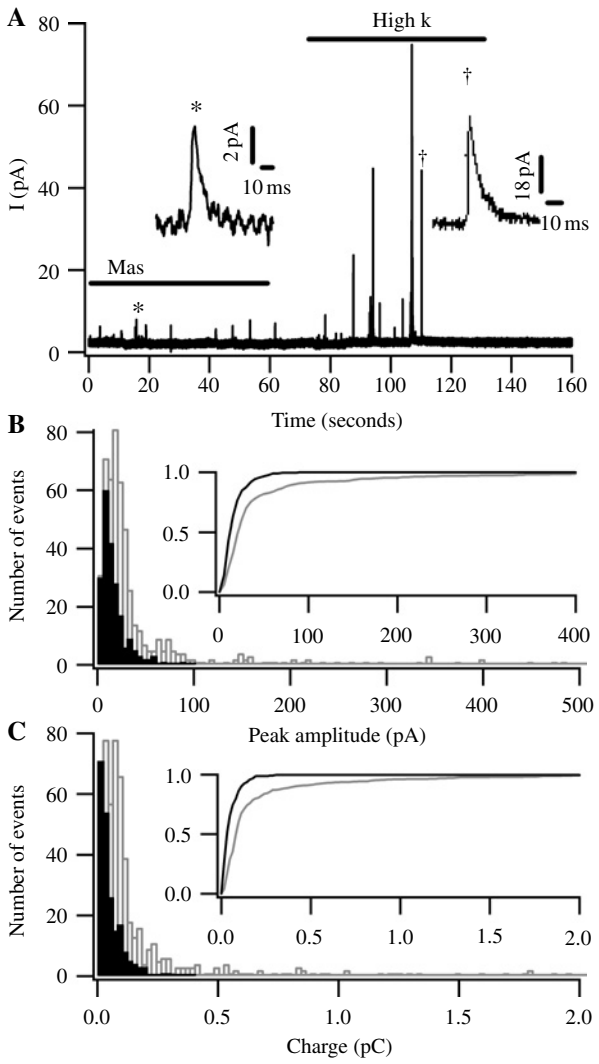

Figure 7: Mastoparan (Mas) induces less release quanta. (A) Amperometric current in a PC12 cell. The cell was first stimulated with 10 μM Mas for 60 seconds followed by 15-second wash with normal external solution, then it is challenged with 120 mM K^+. Example spikes marked with * and † were expanded in the insets, please notice the difference in the scaling. (B) and (C): Distribution of the peak amplitude (B) and charge (C) of amperometric spikes stimulated with high K^+ (empty bar) or Mas (filled bar). Cumulative histograms are compared in the insets. The difference is significant ($p < 0.04$, Kolmogorov–Smirnov test) in both cases.

Discussion

A central role for Ca^{2+} in stimulus-secretion coupling was first proposed more than 30 years ago, particularly through the work of Douglas and Katz (44,45). While we now know how Ca^{2+} interacts with specific Ca^{2+}-binding proteins, we still ignore how these Ca^{2+}-binding proteins initiate membrane fusion. On the contrary, it has become apparent that parallel pathways exist to stimulate exocytosis in the absence of Ca^{2+}, although little is known about the mechanism that mediates Ca^{2+}-independent exocytosis. In the present study, we have taken advantage of the TIRFM technique to monitor single secretory vesicles in live PC12 cells. We employed a slow diffusable marker (NPY-DsRed) to label LDCV and a pH-dependent EGFP conjugated to a vesicular membrane protein (VAMP2-pHluorin) to report fusion. By simultaneous dual-color imaging of single vesicles in live PC12 cells under TIRFM, we studied the mobility of LDCVs in the subplasmalemmal area and their fusion with the plasma membrane stimulated by either Mas or depolarization-evoked Ca^{2+} entry.

Mas is an amphiphilic tetradecapeptide that inserts itself into the phospholipid bilayer of the plasma membrane and displays four positive charges near the inner surface of the membrane. By acting as a structural analogue of the regulatory domain of G-protein-coupled receptors, Mas can mimic the action of these receptors and activate signaling pathways through triggering the guanine nucleotide exchange activity of heterotrimeric G proteins (26), as well as of a low molecular weight G protein (25,27,46). Mas has been widely employed for studying GTP-dependent and Ca^{2+}-independent exocytosis. We have verified in our study that Mas-induced exocytosis is not due to non-specific membrane perturbation via the amphiphilic nature of the peptide but rather is a GTP-dependent membrane fusion process involving the SNARE complex.

We have identified three major differences between Mas- and Ca^{2+}-stimulated exocytosis. Firstly, Mas and Ca^{2+} trigger the fusion from different populations of vesicles. Surprisingly, Mas is inefficient in triggering the exocytosis of predocked vesicles. Instead, we have shown that Mas mainly stimulates the translocation of cytosolic vesicles to the plasma membrane and triggers the subsequent transient fusion of these newcomers. In contrast, Ca^{2+} primarily triggers the exocytosis of predocked vesicles (this study; 35,36). It has been proposed that the docked, primed vesicles undergo inhibition from fusion at resting conditions. This 'fusion clamp' will be relieved only by binding of Ca^{2+} ions to the Ca^{2+} sensor(s). The Ca^{2+}

sensor(s) itself could potentially act as the clamp for fusion (47,48). We now show that this blockade is insensitive to G-protein activation by Mas. Apparently, the fusogenic mechanisms of Mas and Ca^{2+} are different. Although unexpected, our results are consistent with a recent study in which the docked vesicles are triggered to fuse by Ca^{2+} but not by Ba^{2+}, whereas Ba^{2+} preferentially stimulates the fusion of cytoplasmic undocked vesicles (35). By employing a fluorescent timer protein that changes color with maturation, the study proposed that the docked vesicles are newly synthesized and the older vesicles are located deeper in the cytosol. Thus, it is quite likely that vesicles of distinct ages respond differently to Mas. The differential effects of Ca^{2+} and Mas may reflect differences in release mechanisms for vesicles of distinct ages or at different locations.

Secondly, we provide the first evidence to suggest that the Mas-initiated fusion process is different from that triggered by Ca^{2+}. The classical model of exocytosis holds that vesicles flatten into the cell surface and allow their components to mix with the plasma membrane. The possibility that synaptic vesicles release neurotransmitters through incomplete exocytosis, also referred to as 'kiss-and-run', has garnered much attention in recent years (reviewed in 49). The physiological relevance of this type of exocytosis has been attributed to faster vesicle recycling/resupply (50) and to modulation of the amount and type of molecules released (29,51). Despite the importance of regulation of the fusion process (complete versus partial), the mechanistic determination of fusion pore dilation remains unclear. Surprisingly, we have found that the fusion process induced by Ca^{2+} is substantially different from that of GTP-dependent exocytosis in the absence of Ca^{2+}. In Ca^{2+}-induced exocytosis, we observed a single exponential decay ($\tau = 4.5$ seconds) of VAMP2-pHluorin fluorescence after fusion, which could be due to either retreat (38) or re-acidification (52) of vesicles after fusion, or else may be due to lateral diffusion of the fluorescent protein into the plasma membrane (29). We have verified that VAMP2-pHluorin readily diffused into the concentric annuli around the vesicle with similar kinetics after fusion (Figure 6A). Simultaneous monitoring of NPY-DsRed fluorescence (pH-insensitive) of the same vesicle suggests no retreat of the vesicle (Figures 5A and 6A). Thus, the dimming of pHluorin fluorescence is most probably due to loss of the protein into the plasma membrane through lipid mixing after fusion. The diffusion of vesicular membrane proteins and the largely intact nature of the vesicle after fusion are reminiscent of the recently described 'cavicapture' fusion in PC12 cells (29). In contrast, GTP-dependent fusion had a double exponential decay in pHluorin fluorescence as well as in the accompanying NPY-DsRed fluorescence (Figure 6B). Because no diffusion of the fluorescence was observed, the decay in fluorescence is predominantly caused by withdrawal of the vesicle from the plasma membrane and/or rapid re-acidification after fission. The Mas-induced fusion thus resembles the 'kiss-and-run' type of fusion that has been demonstrated from several laboratories using a variety of techniques (52–55). The rapid closure of the fusion pore from Mas-induced fusion will result in a lower catecholamine release, which is consistent with our amperometric data (Figure 7). However, the reduction in quantum size can equally be explained by reduced catecholamine content. It has been reported previously that activation of trimeric G proteins leads to blockade of the vesicular monoamine transporter and thus a reduced loading of vesicles with catecholamines (56).

Thirdly, it appears that not only is the fusion reaction different, but the docking and priming process might also be different for Mas- and Ca^{2+}-triggered exocytosis. Our results indicate that vesicles immediately fuse with the plasma membrane once they attach to the plasma membrane in the presence of Mas. From our imaging data, we estimate that the time required for docking and priming is of the order of 500 ms. In contrast, Ca^{2+}-stimulated exocytosis requires a much longer time (see Figure 6C,D) to reach fusion competence once the vesicle approaches the plasma membrane, which is consistent with previous studies (36,40). Ca^{2+} has been shown to facilitate the priming and docking of vesicles (57,58). The finding that Mas stimulates a much faster docking and priming process than that of Ca^{2+}-evoked exocytosis is hence surprising. The explanation for this apparent difference will rely on further elucidation of the molecular mechanisms of docking and priming and their differential regulation by Ca^{2+} and GTP.

Both monomeric and trimeric GTPases have been suggested to be activated by Mas. The Rho families of low molecular monomeric GTP-binding proteins have been suggested as candidates for Mas action (25,27). The Rho family, which consists of CDC42, Rho, Rac, TC10, and others, are involved in diverse signaling pathways including the regulation of actin cytoskeleton, protein sorting, membrane trafficking, and cell growth control. There is a growing body of evidence to support the possible involvement of the Rho family (Rho, CDC42, Rac) in multiple steps such as vesicle mobilization, docking, and/or membrane fusion (59,60). In addition, Rab GTPases have also been proposed as key regulators for different steps of vesicular transport along the exocytic and endocytic pathways. An emerging role of Rab GTPases has also been recognized in the regulation of vesicle movement on actin tracks (61). Interestingly, we found that latrunculin B, an inhibitor of actin polymerization, blocked Mas-triggered incoming, and fusion of LDCVs (see supplementary Figure 1). Thus, it is quite likely that Mas triggers the translocation and attachment of cytoplasmic vesicles to the plasma membrane via actin tracks, presumably by activation of certain GTPases.

The molecular mechanism by which Mas triggers fusion is also unclear. In particular, the sensor(s) and effector(s) of

GTPase to initiate fusion remain to be identified. Early investigations have implied that heterotrimetric G-protein function in the stimulation of exocytosis (16,62,63). This model was attractive because a direct interaction between βγ subunit and the exocytotic machinery has also been suggested to inhibit presynaptic release downstream of Ca^{2+} entry (64). However, it was subsequently found that the heterotrimetric G proteins are unable to induce exocytosis by themselves (21). It follows that they operate in conjunction with other monomeric GTPases. A recent study has suggested that interaction between RalA and the exocyst complex is essential for GTP-dependent exocytosis (65,66). However, due to the lack of any direct assays of the fusion reaction, it remains to be determined which monomeric GTPase and its effector(s) function in the final fusion step.

The question whether the basic fusion machinery is involved in the GTP-dependent exocytosis remains controversial. The fact that Mas stimulates exocytosis in the effective absence of Ca^{2+} (19,22) and spares the predocked vesicles (this study) appears to suggest that the Ca^{2+} sensor(s) (i.e. synaptotagmin-1) may not be involved. As for the involvement of SNAREs, it has been suggested that VAMP-2 and cellubrevin are essential for Ca^{2+}-induced but not for GTPγS-induced insulin secretion in pancreatic β cells (67). In contrast, a recent study demonstrated that botulinum neurotoxin blocked both GTP- and Ca^{2+}-dependent exocytosis, suggesting their final fusion steps both require SNARE complexes (66). Here, we have demonstrated that Mas-induced exocytosis does require intact SNAP-25. The result not only confirms the universal requirement for SNARE proteins in vesicular fusion but also poses an intriguing question: How could a particular GTP-binding protein convey the signal to the SNARE complexes and initiate fusion? Or alternatively, one could imagine a two-step priming for Ca^{2+}-stimulated exocytosis: the formation of the SNARE complex and the subsequent interaction with synaptotagmin. The interaction with synaptotagmin holds the vesicle from spontaneous fusion, and the blockade can only be released by Ca^{2+}. Mas initiates the SNARE complex formation but prevents further interaction with synaptotagmin (hence the shorter priming time, see Figure 6D). The assembly of the SNARE complex in the absence of synaptotagmin will lead to subsequent fusion in the absence of Ca^{2+}.

We thus propose a tentative model as presented in the supplementary Figure 2 to reconcile the current results. Application of Mas stimulates the translocation and docking of the cytoplasmic vesicles to the plasma membrane. Once the vesicle has docked at the plasma membrane, it immediately undergoes transient fusion (kiss-and-run) with the plasma membrane without entering into a primed (or clamped) state. The transient fusion leads to a small amount of cargo release, and the vesicle returns to the cytoplasmic depot pool soon after the fusion event. The preformed primed vesicles (which are also in a clamped state) will not be triggered to fuse by GTP in the absence of Ca^{2+}. They are, however, triggered to fuse by Ca^{2+}. The fusion pore in the presence of Ca^{2+} remains open for a longer time and has a larger size, which results in larger content release and dispersion of certain membrane proteins. The exocytosed LDCVs are recaptured largely intact after Ca^{2+}-stimulated fusion.

Materials and Methods

Plasmid construction

For the construction of the chimeric protein NPY-DsRed, the NPY-EGFP plasmid was digested with EcoRI and BamHI. The resulting fragment of NPY was then inserted into the EcoRI and BamHI sites of N1-DsRed (Clontech, Palo Alto, CA, USA). BoNT/E light-chain cDNA was subcloned into the pIRES- monomer red fluorescence protein (mRFP) plasmid to express BoNT/E light chain and mRFP (68), separately. The mRFP fluorescence method was used as an indicator of successful transfection.

Cell culture and transfection

PC12 cells were obtained from the American Type Culture Collection (ATCC, Manassas, VA, USA) and were cultured in DMEM (Gibco, Carlsbad, CA, USA) supplemented with 10% horse serum (Gibco) and 5% fetal bovine serum (Gibco) at 37 °C and 5% CO_2. One day after plating, cells were cotransfected with NPY-DsRed and VAMP2-pHluorin using Lipofectamine™ 2000 Transfection Reagent (Invitrogen, Carlsbad, CA, USA). Transfected cells were replated onto coverslips coated with poly L-lysine 1 day after transfection. Experiments were performed 48 h after transfection at room temperature in a standard extracellular saline solution containing 140 mM NaCl, 2.5 mM KCl, 1.3 mM $CaCl_2$, 1 mM $MgCl_2$, and 10 mM Hepes (pH 7.4). The external high K^+ solution used to stimulate the PC12 cells contained (in mM) 37 NaCl, 105 KCl, 5 $CaCl_2$, 2 $MgCl_2$, and 10 HEPES (pH 7.4). Mas was prepared as 1 mM stock solution and diluted to 10 μM in Ca^{2+}- and Mg^{2+}-free external solution containing 140 mM NaCl, 2.8 mM KCl, 10 mM HEPES, 1 mM EGTA, and 10 mM glucose (pH = 7.4). To examine the co-localization of VAMP2-pHluorin with NPY-DsRed, we perfused transfected cells with NH_4Cl solution prepared by substituting 50 mM NaCl with 50 mM NH_4Cl in the standard bath solution. Unless otherwise stated, all compounds were purchased from Sigma.

Imaging collection and analysis

The TIRFM setup was constructed based on the prismless and through-the-lens configuration as previously described (69). Briefly, a condenser coupling multiple lasers was attached to the back port of an IX81-inverted automatic microscope (Olympus, Tokyo, Japan) equipped with a ×100 objective lens (NA = 1.45, Zeiss, Germany). The 488-nm laser line was selected using AOTF for simultaneous illumination of EGFP and DsRed. An appropriate dichroic mirror (DC488nm) and emission filter (LP505nm) were placed in the light path. Images were collected at 3–5 Hz using Cascade 650 (Roper Scientific, Tucson, AZ, USA) at the right lateral port of the microscope after a GFP/DsRed dual-view microimager (Optical Insights, Tucson, AZ, USA). We calculated the penetration depth of the evanescent field (d = 138 nm) by measuring the incidence angle with a prism ($n = 1.5218$) with a 488-nm laser beam. Imaging was controlled using Metamorph (Universal Imaging, Downingtown, PA, USA) and analyzed in MatLab (Math Works, Natick, MA, USA) or Igor Pro (WaveMetrics, Lake Oswego, OR, USA).

Data analysis

Fluorescent spots were considered to be 'secretory vesicles' if their intensity was three times above the background fluctuations, and they had a full width at half-maximum diameter below 0.5 μm (37). We used two concentric

circles (13 and 20 pixels with a pixel size of 74 nm, corresponding to approximately 1.0 and 1.5-μm diameter), centered on selected vesicles, to characterize the evolution of fluorescence over time of single vesicles on background-subtracted images. Fluorescence of individual vesicles was measured as the mean brightness of the inner circle. Abrupt upward deflections in pHluorin fluorescence exceeding five times the standard deviation of the fluorescence fluctuation were considered as fusion events. Additionally, we took the dissipation of the average fluorescence in the concentric annulus as a reporter of release of vesicular fluorophores. Throughout our dual-color experiments, same regions defined for VAMP2-pHluorin analysis were transferred to the corresponding positions of the red image, and the above procedures were carried out for parallel analysis of the co-localized NPY-DsRed fluorescence.

To analyze the mobility of single vesicles, we fitted a 2-D Gaussian distribution to the single-vesicle data. This algorithm is proven to be an effective approach in tracking single fluorescent particles at low signal-to-noise levels (37,38). The lateral co-ordinates of the vesicle were taken from the peak of the Gaussian fit. The relative movement in the z position (ΔZ_n) from time point ($n-1$) to (n) can be calculated from the following formula (38):

$$\Delta Z_n = Z_n - Z_{n-1} = -d\,ln\,(F_n/F_{n-1}) \quad (1)$$

where F_n and F_{n-1} are background corrected fluorescence at time point (n) and ($n-1$), respectively, and d is the penetration depth. The penetration depth was verified frequently by measuring the incidence angle before the experiments. The MSD for each vesicle was calculated from NPY-DsRed-labeled vesicles as follows:

$$\mathrm{MSD}(t) = \frac{1}{L-n}\sum_{s=0}^{L-n-1}\left(r(s+n) - r(s)\right)^2 \quad (2)$$

where $n = t/\Delta t$; Δt is the time interval between two successive TIRFM-recorded images, L is the total number of images in a recorded sequence, and $r(s)$ is the 3-D position of vesicle in frame s. The data were fit according to the equation $MSD(\Delta t) = 6D^{(3)}\Delta t$ as described previously (37,38), which yielded the 3-D diffusion coefficient $D^{(3)}$ from the best least-squares fit.

Ca^{2+}-uncaging and $[Ca^{2+}]_i$ measurement

Homogenous $[Ca^{2+}]_i$ elevations were generated by the photolysis of caged Ca^{2+} (DMN), as previously described (70). Pipette solutions consisted of 110 mM Cs-glutamate, 5 mM DMN, 8 mM NaCl, 3.6 mM $CaCl_2$, 2 mM MgATP, 0.3 mM GTP, 0.2 mM furaptra, and 35 mM Hepes, adjusted to pH 7.2 with either HCl or CsOH. We estimated basal $[Ca^{2+}]_i$ levels of the order of approximately 300 nM by fura-2. $[Ca^{2+}]_i$ levels were calculated from the 340/380-nm fluorescence ratio according to the following equation (71): $[Ca^{2+}]_i = \mathrm{Keff} \times (R - \mathrm{Rmin})/(\mathrm{Rmax} - R)$, where Keff, Rmin, and Rmax are constants obtained from intracellular calibration as previously described (70).

Cm measurement

We performed whole-cell recordings using sylgard-coated 2–3 MΩ pipettes. Series resistances of between 4 and 12 MΩ were included in the analysis. An EPC-10 patch-clamp amplifier (HEKA, Lambrecht, Germany) was used with PULSE+LOCK-IN software. For capacitance measurements, a 1042-Hz, 40-mV peak-to-peak sinusoidal voltage stimulus was superimposed onto a holding potential of −70 mV. Currents were filtered at 2.9 kHz and sampled at 25 kHz. The capacitance traces were imported into IGOR Pro and were fitted with a triple exponential function:

$$f(t) = A_0 + \sum_{i=1}^{3} A_i\left((1 - \exp\left(-\frac{t-t_0}{\tau_i}\right)\right) for\ t > t_0 \quad (3)$$

where A_0 is the capacitance of the cell before the flash stimulation at t_0. The amplitudes (A_i) and time constants (τ_i) of the two faster exponentials define the size and release kinetics of the fast- and slow-burst component, respectively. The third exponential corresponds to the component of sustained release and was quantified by the rate of Cm increase.

Amperometric recordings of catecholamine release

Amperometric recordings were performed with polypropylene insulated carbon fiber (Thornel T-300, diameter 7 μm, Amoco Performance Products, Greenville, SC, USA) electrodes held at +650 mV using an EPC-9 amplifier (HEKA). Signals were filtered at 500 Hz and sampled at 1 kHz. Amperometric events were viewed and analyzed with Minianalyses (Synaptosft., Decatur, GA, USA).

The measurement of high K^+-stimulated catecholamine release was performed in the normal extracellular solution. High K^+ buffer consisted of 25 mM NaCl, 120 mM KCl, 5 mM $CaCl_2$, 0.7 mM $MgCl_2$, 10 mM Hepes, and 10 mM glucose. The Mas-stimulated secretion was recorded in the Ca^{2+} and Mg^{2+}-free external solution. The external solutions were adjusted to pH 7.4 with either HCl or NaOH.

Statistics

For normally distributed data, population averages were given as mean and SEM, and statistical significance was tested with Student's *t*-test. Statistical significance between skewed distributions was assessed with Kolmogorov–Smirnov test.

Acknowledgments

We thank Drs W Almers for providing the NPY-EGFP plasmids, J Rothman for VAMP2-pHluorin, RY Tsien for mRFP, and TFJ Martin for BoNT/E light-chain plasmids. We are grateful for critical reading of the manuscript by Dr Mark Bartlam. This work was supported by grants from the National Science Foundation of China (30025023, 30270363, 30470448, 30130230), the Major State Basic Research Program of China (G1999054000, 2004CB720000), the CAS Project (KSCX2-SW-224, Y2004018), the Li Foundation, and the Sinogerman Scientific Center. The laboratory of TX belongs to a Partner Group Scheme of the Max Planck Institute for Biophysical Chemistry, Göttingen.

Supplementary Material

Figure S1. Cumulative numbers of fusion events stimulated by mastoparan (Mas) were plotted against time from cells with (TG + Mas, open circle) or without (Mas, filled circle) pretreatment of thapsigargin (TG, 2 μM for 15 min). Also compared are Mas-induced fusion events from cells pretreated with latrunculin B (5 μM) for 5 min (LB + Mas).

Figure S2. Tentative model for the Ca^{2+}- and GTP-dependent exocytosis. Ca^{2+} and activated G proteins control exocytosis via two different mechanisms. G-protein activation triggers translocation and docking of vesicles and subsequent transient fusion. Through a brief opening of the fusion pore, only a small amount of content is released. Whereas the primed vesicles are spared by GTP, they are triggered to fuse by Ca^{2+}. Fusion of large dense core granule induced by Ca^{2+} has a longer and larger opening of the fusion pore, which results in larger content release and also partial diffusion of certain vesicular membrane proteins.

These materials are available as part of the online article from http://www.blackwell-synergy.com

References

1. Sollner T, Bennett MK, Whiteheart SW, Scheller RH, Rothman JE. A protein assembly-disassembly pathway in vitro that may correspond to sequential steps of synaptic vesicle docking, activation, and fusion. Cell 1993;75:409–418.
2. Rizo J, Sudhof TC. SNAREs and Munc18 in synaptic vesicle fusion. Nat Rev Neurosci 2002;3:641–653.
3. Chen YA, Scales SJ, Scheller RH. Sequential SNARE assembly underlies priming and triggering of exocytosis. Neuron 2001;30:161–170.
4. Lonart G, Sudhof TC. Assembly of SNARE core complexes prior to neurotransmitter release sets the readily releasable pool of synaptic vesicles. J Biol Chem 2000;275:27703–27707.
5. Xu T, Binz T, Niemann H, Neher E. Multiple kinetic components of exocytosis distinguished by neurotoxin sensitivity. Nat Neurosci 1998;1:192–200.
6. Xu T, Rammner B, Margittai M, Artalejo AR, Neher E, Jahn R. Inhibition of SNARE complex assembly differentially affects kinetic components of exocytosis. Cell 1999;99:713–722.
7. Brose N, Petrenko AG, Sudhof TC, Jahn R. Synaptotagmin: a calcium sensor on the synaptic vesicle surface. Science 1992;256:1021–1025.
8. Fernandez-Chacon R, Konigstorfer A, Gerber SH, Garcia J, Matos MF, Stevens CF, Brose N, Rizo J, Rosenmund C, Sudhof TC. Synaptotagmin I functions as a calcium regulator of release probability. Nature 2001;410:41–49.
9. Jahn R, Lang T, Sudhof TC. Membrane fusion. Cell 2003;112:519–533.
10. Fernandez JM, Neher E, Gomperts BD. Capacitance measurements reveal stepwise fusion events in degranulating mast cells. Nature 1984;312:453–455.
11. Nusse O, Lindau M. The dynamics of exocytosis in human neutrophils. J Cell Biol 1988;107:2117–2123.
12. Gomperts BD. Involvement of guanine nucleotide-binding protein in the gating of Ca^{2+} by receptors. Nature 1983;306:64–66.
13. Bittner MA, Holz RW, Neubig RR. Guanine nucleotide effects on catecholamine secretion from digitonin-permeabilized adrenal chromaffin cells. J Biol Chem 1986;261:10182–10188.
14. Burgoyne RD, Handel SE. Activation of exocytosis by GTP analogues in adrenal chromaffin cells revealed by patch-clamp capacitance measurement. FEBS Lett 1994;344:139–142.
15. Okano K, Monck JR, Fernandez JM. GTP gamma S stimulates exocytosis in patch-clamped rat melanotrophs. Neuron 1993;11:165–172.
16. Tse FW, Tse A. Stimulation of Ca(2+)-independent exocytosis in rat pituitary gonadotrophs by G-protein. J Physiol 2000;526 (Pt 1):99–108.
17. Regazzi R, Li G, Ullrich S, Jaggi C, Wollheim CB. Different requirements for protein kinase C activation and Ca^{2+}-independent insulin secretion in response to guanine nucleotides. Endogenously generated diacylglycerol requires elevated Ca^{2+} for kinase C insertion into membranes. J Biol Chem 1989;264:9939–9944.
18. Chen D, Lemons PP, Schraw T, Whiteheart SW. Molecular mechanisms of platelet exocytosis: role of SNAP-23 and syntaxin 2 and 4 in lysosome release. Blood 2000;96:1782–1788.
19. Kumakura K, Ohara-Imaizumi M, Muramatsu S, Terakawa S, Kanno T. Mastoparan evokes exocytosis without Ca^{2+} movement in adrenal chromaffin cells. Jpn J Physiol 1993;43 (Suppl. 1):S109–S113.
20. Wheeler-Jones CP, Saermark T, Kakkar VV, Authi KS. Mastoparan promotes exocytosis and increases intracellular cyclic AMP in human platelets. Evidence for the existence of a Ge-like mechanism of secretion. Biochem J 1992;281 (Pt 2):465–472.
21. Pinxteren JA, O'Sullivan AJ, Tatham PE, Gomperts BD. Regulation of exocytosis from rat peritoneal mast cells by G protein beta gamma-subunits. EMBO J 1998;17:6210–6218.
22. Komatsu M, McDermott AM, Gillison SL, Sharp GW. Mastoparan stimulates exocytosis at a Ca(2+)-independent late site in stimulus-secretion coupling. Studies with the RINm5F beta-cell line. J Biol Chem 1993;268:23297–23306.
23. Straub SG, James RF, Dunne MJ, Sharp GW. Glucose augmentation of mastoparan-stimulated insulin secretion in rat and human pancreatic islets. Diabetes 1998;47:1053–1057.
24. Joyce-Brady M, Rubins JB, Panchenko MP, Bernardo J, Steele MP, Kolm L, Simons ER, Dickey BF. Mechanisms of mastoparan-stimulated surfactant secretion from isolated pulmonary alveolar type 2 cells. J Biol Chem 1991;266:6859–6865.
25. Daniel S, Noda M, Cerione RA, Sharp GW. A link between Cdc42 and syntaxin is involved in mastoparan-stimulated insulin release. Biochemistry 2002;41:9663–9671.
26. Higashijima T, Uzu S, Nakajima T, Ross EM. Mastoparan, a peptide toxin from wasp venom, mimics receptors by activating GTP-binding regulatory proteins (G proteins). J Biol Chem 1988;263:6491–6494.
27. Koch G, Haberman B, Mohr C, Just I, Aktories K. Interaction of mastoparan with the low molecular mass GTP-binding proteins Rho/Rac. FEBS Lett 1991;291:336–340.
28. Tsuboi T, Rutter GA. Multiple forms of 'kiss-and-run' exocytosis revealed by evanescent wave microscopy. Curr Biol 2003;13:563–567.
29. Taraska JW, Perrais D, Ohara-Imaizumi M, Nagamatsu S, Almers W. Secretory granules are recaptured largely intact after stimulated exocytosis in cultured endocrine cells. Proc Natl Acad Sci USA 2003;100:2070–2075.
30. Miesenbock G, De Angelis DA, Rothman JE. Visualizing secretion and synaptic transmission with pH-sensitive green fluorescent proteins. Nature 1998;394:192–195.
31. Lang T, Wacker I, Steyer J, Kaether C, Wunderlich I, Soldati T, Gerdes HH, Almers W. Ca^{2+}-triggered peptide secretion in single cells imaged with green fluorescent protein and evanescent-wave microscopy. Neuron 1997;18:857–863.
32. Shaner NC, Campbell RE, Steinbach PA, Giepmans BN, Palmer AE, Tsien RY. Improved monomeric red, orange and yellow fluorescent proteins derived from Discosoma sp. red fluorescent protein. Nat Biotechnol 2004;22:1567–1572.
33. Han W, Li D, Stout AK, Takimoto K, Levitan ES. Ca^{2+}-induced deprotonation of peptide hormones inside secretory vesicles in preparation for release. J Neurosci 1999;19:900–905.
34. Niemann H, Blasi J, Jahn R. Clostridial neurotoxins: new tools for dissecting exocytosis. Trends Cell Biol 1994;4:179–185.
35. Duncan RR, Greaves J, Wiegand UK, Matskevich I, Bodammer G, Apps DK, Shipston MJ, Chow RH. Functional and spatial segregation of secretory vesicle pools according to vesicle age. Nature 2003;422:176–180.
36. Steyer JA, Horstmann H, Almers W. Transport, docking and exocytosis of single secretory granules in live chromaffin cells. Nature 1997;388:474–478.
37. Li D, Xiong J, Qu A, Xu T. Three-dimensional tracking of single secretory granules in live PC12 cells. Biophys J 2004;87:1991–2001.
38. Oheim M, Stuhmer W. Tracking chromaffin granules on their way through the actin cortex. Eur Biophys J 2000;29:67–89.
39. Steyer JA, Almers W. Tracking single secretory granules in live chromaffin cells by evanescent-field fluorescence microscopy. Biophys J 1999;76:2262–2271.
40. Oheim M, Loerke D, Stuhmer W, Chow RH. Multiple stimulation-dependent processes regulate the size of the releasable pool of vesicles. Eur Biophys J 1999;28:91–101.
41. Sorensen JB. Formation, stabilisation and fusion of the readily releasable pool of secretory vesicles. Pflugers Arch 2004;448:347–362.
42. Zenisek D, Steyer JA, Almers W. Transport, capture and exocytosis of single synaptic vesicles at active zones. Nature 2000;406:849–854.

43. Holz RW, Axelrod D. Localization of phosphatidylinositol 4,5-P(2) important in exocytosis and a quantitative analysis of chromaffin granule motion adjacent to the plasma membrane. Ann NY Acad Sci 2002;971:232–243.
44. Douglas WW, Rubin RP. Mechanism of nicotinic action at the adrenal medulla: calcium as a link in stimulus-secretion coupling. Nature 1961;192:1087–1089.
45. Katz B, Miledi R. Ionic requirements of synaptic transmitter release. Nature 1967;215:651.
46. Amin RH, Chen HQ, Veluthakal R, Silver RB, Li J, Li G, Kowluru A. Mastoparan-induced insulin secretion from insulin-secreting betaTC3 and INS-1 cells: evidence for its regulation by Rho subfamily of G proteins. Endocrinology 2003;144:4508–4518.
47. DiAntonio A, Schwarz TL. The effect on synaptic physiology of synaptotagmin mutations in Drosophila. Neuron 1994;12:909–920.
48. Morimoto T, Popov S, Buckley KM, Poo MM. Calcium-dependent transmitter secretion from fibroblasts: modulation by synaptotagmin I. Neuron 1995;15:689–696.
49. An S, Zenisek D. Regulation of exocytosis in neurons and neuroendocrine cells. Curr Opin Neurobiol 2004;14:522–530.
50. Harata N, Pyle JL, Aravanis AM, Mozhayeva M, Kavalali ET, Tsien RW. Limited numbers of recycling vesicles in small CNS nerve terminals: implications for neural signaling and vesicular cycling. Trends Neurosci 2001;24:637–643.
51. Choi S, Klingauf J, Tsien RW. Fusion pore modulation as a presynaptic mechanism contributing to expression of long-term potentiation. Philos Trans R Soc Lond B Biol Sci 2003;358:695–705.
52. Li Z, Burrone J, Tyler WJ, Hartman KN, Albeanu DF, Murthy VN. Synaptic vesicle recycling studied in transgenic mice expressing synaptopHluorin. Proc Natl Acad Sci USA 2005;102: 6131–6136.
53. Henkel AW, Almers W. Fast steps in exocytosis and endocytosis studied by capacitance measurements in endocrine cells. Curr Opin Neurobiol 1996;6:350–357.
54. Albillos A, Dernick G, Horstmann H, Almers W, Alvarez de Toledo G, Lindau M. The exocytotic event in chromaffin cells revealed by patch amperometry. Nature 1997;389:509–512.
55. Aravanis AM, Pyle JL, Tsien RW. Single synaptic vesicles fusing transiently and successively without loss of identity. Nature 2003;423: 643–647.
56. Ahnert-Hilger G, Nurnberg B, Exner T, Schafer T, Jahn R. The heterotrimeric G protein Go2 regulates catecholamine uptake by secretory vesicles. EMBO J 1998;17:406–413.
57. von Ruden L, Neher E. A Ca-dependent early step in the release of catecholamines from adrenal chromaffin cells. Science 1993;262: 1061–1065.
58. Smith C, Moser T, Xu T, Neher E. Cytosolic Ca^{2+} acts by two separate pathways to modulate the supply of release-competent vesicles in chromaffin cells. Neuron 1998;20:1243–1253.
59. Symons M, Rusk N. Control of vesicular trafficking by Rho GTPases. Curr Biol 2003;13:R409–R418.
60. Gasman S, Chasserot-Golaz S, Popoff MR, Aunis D, Bader MF. Involvement of Rho GTPases in calcium-regulated exocytosis from adrenal chromaffin cells. J Cell Sci 1999;112 (Pt 24):4763–4771.
61. Seabra MC, Coudrier E. Rab GTPases and myosin motors in organelle motility. Traffic 2004;5:393–399.
62. Aridor M, Rajmilevich G, Beaven MA, Sagi-Eisenberg R. Activation of exocytosis by the heterotrimeric G protein Gi3. Science 1993;262: 1569–1572.
63. Watson EL. GTP-binding proteins and regulated exocytosis. Crit Rev Oral Biol Med 1999;10:284–306.
64. Blackmer T, Larsen EC, Takahashi M, Martin TF, Alford S, Hamm HE. G protein betagamma subunit-mediated presynaptic inhibition: regulation of exocytotic fusion downstream of Ca^{2+} entry. Science 2001;292: 293–297.
65. Moskalenko S, Henry DO, Rosse C, Mirey G, Camonis JH, White MA. The exocyst is a Ral effector complex. Nat Cell Biol 2002;4:66–72.
66. Wang L, Li G, Sugita S. RalA-exocyst interaction mediates GTP-dependent exocytosis. J Biol Chem 2004;279:19875–19881.
67. Regazzi R, Wollheim CB, Lang J, Theler JM, Rossetto O, Montecucco C, Sadoul K, Weller U, Palmer M, Thorens B. VAMP-2 and cellubrevin are expressed in pancreatic beta-cells and are essential for Ca(2+) but not for GTP gamma S-induced insulin secretion. EMBO J 1995;14: 2723–2730.
68. Campbell RE, Tour O, Palmer AE, Steinbach PA, Baird GS, Zacharias DA, Tsien RY. A monomeric red fluorescent protein. Proc Natl Acad Sci USA 2002;99:7877–7882.
69. Xia S, Xu L, Bai L, Xu ZQ, Xu T. Labeling and dynamic imaging of synaptic vesicle-like microvesicles in PC12 cells using TIRFM. Brain Res 2004;997:159–164.
70. Xu T, Naraghi M, Kang H, Neher E. Kinetic studies of Ca^{2+} binding and Ca^{2+} clearance in the cytosol of adrenal chromaffin cells. Biophys J 1997;73:532–545.
71. Grynkiewicz G, Poenie M, Tsien RY. A new generation of Ca^{2+} indicators with greatly improved fluorescence properties. J Biol Chem 1985;260:3440–3450.